Propagating and localized vibrational modes in Ni-Zr glasses

1994 J. Phys.: Condens. Matter 6 4631

(http://iopscience.iop.org/0953-8984/6/25/003)

J. Phys.: Condens. Matter 6 (1994) 4631–4654. Printed in the UK

Propagating and localized vibrational modes in Ni–Zr glasses

J Hafner and M Krajčí

Institut für Theoretische Physik, TU Wien, Wiedner Hauptstraße 8–10, A-1040 Wien, Austria

Received 17 February 1994, in final form 13 April 1994

Abstract. Numerical investigations of the vibrational eigenmodes of amorphous Ni_xZr_{100-x} alloys are presented. Structural models are prepared by molecular dynamics simulations of the quenching processes, based on interatomic forces derived using a tight-binding-bond approach. The vibrational properties are investigated via a direct diagonalization of the dynamical matrix for $N = 729$-atom models, and via recursion calculations of the vibrational spectral functions, partial and total dynamical structure factors and vibrational densities of states for large $N = 2916$-atom models. The static structure of the Ni_xZr_{100-x} glasses is characterized by a pronounced chemical and topological short-range order (SRO). We investigate in detail the manifestation of the SRO in the partial dynamic spectral functions and structure factors $S_{IJ}(k, \omega)$. We discuss the possibility of measuring partial dynamic structure factors using inelastic neutron scattering and demonstrate that our results are in good agreement with the existing experimental data on the total dynamical structure factors. We show that, although most eigenmodes are extended, localized modes can be found at the upper and lower edges of the frequency spectrum. Of particular interest is the prediction of low-energy localized modes, which have a profound influence on the low-temperature thermodynamic properties.

1. Introduction

In recent years considerable progress has been made in our understanding of elementary excitations in disordered materials [1, 2]. A complete description of structural modes is required as a basis for an understanding of certain physical phenomena that are thought to be characteristic of the glassy state: the glass transition [3] (which is essentially dynamical in origin), the electrical resistivity [4, 5], the Eliashberg function [6] of amorphous metals etc. In any case, a detailed knowledge of the spectrum of vibrational excitations and of the dynamical structure factors is necessary. Of particular importance is the determination of dispersion laws. It has been shown that simple glasses (like metallic glasses [7–10] or Lennard-Jones glasses [11, 12]) support propagating collective excitations up to rather high wavenumbers. The dispersion relation of these modes (for which we shall use the term 'phonon', although of course it is strictly applicable only to crystalline systems) is linear in the long-wavelength regime, with a slope corresponding to the velocity of sound. At larger wavenumbers the dispersion relation bends over and goes through a maximum and then through a minimum at values of $|k|$ close to $Q_p/2$ and Q_p (the position of the first peak in the static structure factor $S(k)$). A similar form of the dispersion law is observed in He-II and also in some simple liquids [13] (notably liquid metals [14]). It has been shown [15] that the origin of the dispersion minimum is best described in terms of a diffuse-Umklapp scattering process, the sharp first peak at $k = Q_p$ in the static structure factor of the glass playing the role of a reciprocal lattice vector and $Q_p/2$ the role of a pseudo-Brillouin-zone boundary. This theme has been elaborated in a number of simple models [16, 17].

0953-8984/94/254631+24$19.50

The 'phonon-like' excitations determine the properties of glasses at temperatures above 10 K. At temperatures below 1 K, the properties of glasses differ strongly from those of the crystalline phase of the same material. These differences can be described satisfactorily by the well known tunnelling model [18–20]. In the range 1–10 K the anomalous behaviour of the glassy materials may be explained only by assuming the existence of additional modes coexisting with the sound waves [20, 21]. There is experimental evidence [22] that at least some of these additional modes are localized low-frequency harmonic vibrations. A number of attempts have been made to elucidate the structural origin of these localized soft modes and their possible correlation with the tunnelling states [23–25].

To date, most studies (experimental, computational or theoretical) have been performed on simple model systems whose structure may be described, at least within a certain approximation, in terms of the dense random packing of soft spheres (inverse power potentials [25], Lennard-Jones systems [11, 12, 23]; this also includes binary metallic glasses [7–10] such as $Mg_{70}Zn_{30}$ or $Ca_{70}Mg_{30}$ which show only weak chemical or topological short-range order). In reality, glasses conforming with this simplifying picture are the exception rather than the rule. Many of the most stable metallic glasses formed in binary transition-metal systems (e.g. Ni–Zr, Ni–Y, Fe–Y and so on) or in transition-metal–metalloid systems (e.g. Fe–B, Ni–P and so on) show strong chemical and topological short-range order (SRO). The description of the SRO requires the determination of the three partial static structure factors $S_{ij}(k)$. Experimentally, this may be achieved using various diffraction techniques (neutron diffraction on isotopically substituted samples producing the most reliable results [26]). Computer experiments are successful if they are based on sufficiently realistic interatomic force fields [27, 28]. Both laboratory and computer experiments point to a pronounced similarity of the SRO in the glassy and crystalline states. The open question is whether this similarity is also reflected in the dynamical properties.

This is precisely the problem we address in this paper. We present a detailed numerical investigation of the dynamical properties of Ni_xZr_{100-x} glasses. Model structures are prepared by a simulated molecular-dynamics quench based on interatomic forces derived by a hybridized nearly-free-electron tight-binding-bond approach [27], leading to partial static structure factors in good agreement with neutron-diffraction data [29–31]. The vibrational density of states and Bloch spectral functions for propagating collective excitations are calculated using a recursion technique [9, 10, 32, 33]. The partial spectral functions may be used to derive the partial dynamical structure factors $S_{IJ}(k, \omega)$ and the inelastic neutron scattering law $S(k, \omega)$. Localization of vibrational excitations is characterized by the inverse participation ratio calculated in terms of the eigenvectors of the dynamical excitations, obtained by direct diagonalization of the dynamical matrix. Our results show that certain features in the partial static structure factors $S_{IJ}(k)$ characterizing the SRO (prepeaks, shoulders in the higher-order peaks) also appear in the partial dynamical structure factors $S_{IJ}(k, \omega)$, at least for not-too-high frequencies. The 'dynamical' prepeaks show dispersion and merge at intermediate frequencies with the sound-wave peaks. At these frequencies the peaks in the dynamical structure factors become very broad, indicating that propagating modes are strongly overdamped in this frequency regime. At still higher frequencies sharp structures in the $S_{IJ}(k, \omega)$ reappear. At the highest vibrational frequencies, the sound-wave peak and the main structural peak merge at a $k \sim Q_p/2$. Again, the pronounced differences in the partial dynamical structure factors reflect the SRO in the glass. We also calculate the inelastic neutron-scattering law and demonstrate that at the level of composite (neutron-weighted) dynamical structure factors there is a good agreement with the few available experimental data [34]. We also discuss the possibility for an experimental determination of partial dynamic structure factors using isotope-substitution techniques.

Our calculations show that, although most eigenmodes are extended, the modes at the upper edge of the spectrum and some low-energy modes are localized, i.e. the atomic displacements are largest for a small number of isolated atoms. The high-frequency modes are associated with locally constrained configurations whose existence is the inevitable consequence of the rapid quenching process. More interesting is the small number of low-frequency localized modes that are found in all models, irrespective of composition. The localized low-frequency properties dominate the low-temperature anomalies of the glasses. The possible origin of the modes and the relation with the soft-potential model [24, 25] is discussed.

2. Generation and characterization of the structural model

2.1. Interatomic force field

The basic assumption of the hybridized nearly-free-electron tight-binding-bond approach [27] is that the total energy may be divided into contributions from the strongly bonded d electrons and the much more mobile s electrons. The s-electron contribution to total energy and interatomic forces is calculated using standard pseudopotential theory [35, 36]. The d-electron contribution may be written within local-density theory in terms of a repulsive pairwise interaction containing the electrostatic, exchange–correlation and non-orthogonality contributions to the total energy and a covalent bond-energy E_{dbond} resulting from the formation of the d band [37]. s–d hybridization is considered in a lowest-order approximation by fixing the correct numbers of s and d electrons. Assuming the d orbitals in amorphous or liquid metals to be degenerate and neglecting the directionality of the d bands, E_{dbond} can be written in a two-centre orthogonal tight-binding approximation as [38]

$$E_{\text{dbond}} = \frac{1}{2N} \sum_{\substack{i,j \\ i \neq j}} t_{ij}(R_{ij}) \Theta_{ij} \tag{1}$$

where t_{ij} is the transfer integral for d orbitals centred at the sites i and j (distance R_{ij}) and Θ_{ij} is the bond order counting the difference in the number of electrons in the bonding and antibonding states formed by the orbitals at sites i and j. Equation (1) describes only formally a pair interaction. In general, the dependence of the bonding forces on the atomic environment of the bond enters via the bond order. For disordered materials the problem is that the atomic structure is not known *a priori*, but has to be calculated on the basis of the interatomic forces. Hence the forces must be calculated on an appropriately chosen reference structure. For amorphous metals it has been shown that a Bethe lattice (where the local atomic environment is characterized by a mean coordination number and an average bond length) is a sufficiently realistic reference system and allows in addition for an analytic calculation of the bond order. For monatomic materials, the bonding forces are proportional to the inverse square root of the effective coordination number, hence the approach is similar in spirit to the Finnis–Sinclair potentials [39] (but requires no adjustable parameters). In binary systems the character of the bonding forces is determined by [27, 28] (i) the difference $\Delta\epsilon_d$ in the position of the atomic d levels (adjusted such as to ensure local charge neutrality) in relation to the average d-band width $\overline{W_d}$ and (ii) the filling of the d band. If $\Delta\epsilon_d$ is comparable to or only slightly smaller than $\overline{W_d}$ (for example, in Cu–Y, Ni–Y, Ni–Zr), the alloy is close to the split-band limit with the lower part of the band dominated by the 'late' transition metal (Cu, Ni, ...) and the upper part dominated

by the early transition metal (Y, Zr, ...). In this case the bond-order for unlike-atom pairs is largest, and the pair forces show a strong preference for heterocoordination. In addition the minimum in the unlike-atom potential occurs at shorter distances, resulting in very short A–B bonds. The preference for strong and short heteroatomic bonds is largest if the Fermi level falls into the pseudogap separating the two parts of the d band. Conversely, if $\Delta\epsilon_d \ll W_d$, the d electrons form a common band with little structure and the pair forces are essentially additive or show a weak tendency to segregation (due to size effects). For details, we refer the reader to [27].

2.2. *Simulated molecular dynamics quench*

The structure of the amorphous alloys has been generated by a simulated molecular dynamics quench. The starting configuration consists of a face-centred cubic lattice with a random distribution of the two atomic species. In the first step, the system is molten at a temperature several hundred degrees above the liquidus line. After reaching equilibrium, the liquid alloy is compressed isothermally to the density of the glassy phase, followed by an isochoric quench to room temperature at a rate of $\dot{T} \simeq 10^{14}\,\mathrm{K\,s^{-1}}$. Data for the calculation of the static structure factors are sampled over long runs of several thousand timesteps (technical details of the molecular dynamics routines are given in [40,41]). To prepare the equilibrium configuration for the recursion calculation of the dynamical properties, the system is further quenched to nearly 0 K and a force-free configuration is determined by a conjugate-gradient minimization of the total energy. The simulations were performed for large ensembles of $N = 2916$ atoms (serving as the basis for the recursion calculations) and for smaller ensembles of $N = 729$ atoms (they are the starting configurations for the exact diagonalization of the dynamical matrix). Ni_xZr_{100-x} alloys with compositions $x = 25$, 35, 50 and 65 and number densities of $n = 0.0491\,\text{Å}^{-3}$, $n = 0.0527\,\text{Å}^{-3}$, $n = 0.0584\,\text{Å}^{-3}$ and $n = 0.0655\,\text{Å}^{-3}$ (taken from experiment [29–31,34]) have been considered in this study.

2.3. *Glass structure*

The static structure of amorphous Ni–Zr alloys has been described in detail in [27] (based on MD quenches for $N = 1372$-atom ensembles). Here we recapitulate only the main results.

(i) The non-additivity of the pair potentials leads to a strong CSRO at all compositions. In the partial static structure factors $S_{IJ}(k)$, the chemical ordering is reflected by a pronounced prepeak in the like-atom structure factors $S_{II}(k)$. For the minority species the CSRO prepeak has an even larger amplitude than the main structural peak arising from density fluctuations. For comparison, the partial static structure factors are included in the graphs representing the partial dynamic structure factors (see figure 3(*a*)–(*c*)).

(ii) The very short bond length for unlike-atom bonds, together with the rather large size ratio ($R_{Zr}/R_{Ni} = 1.323$ in terms of the atomic radii of the pure metals) leads to a strong topological short-range order (TSRO) as well. The TSRO is similar in the crystalline and amorphous phases: in the Zr-rich alloys ($x \geqslant 50$) the local order is of a trigonal–prismatic type, the dominant local motif is a distorted trigonal prism of six Zr atoms centred by an Ni atom. The crystalline Ni–Zr compounds with the $CuAl_2$ and BCr structures [42] are built of these units in corner-, edge- and face-sharing arrangements. Evidence for their existence in the amorphous alloys comes from the coincidence of the crystalline interatomic distances with the peaks in the pair-correlation functions, and from the analysis of the bond-angle distribution functions (especially the bond angles formed by Ni–Ni–Ni triplets give a clear signal) [27]. With increasing Ni content the character of the TSRO gradually changes to a

tetrahedrally close-packed type. Tetrahedral close packing is also realized in the Ni-rich intermetallic compounds (e.g. Ni_2Zr with the structure of the cubic Laves phase Cu_2Mg, and Ni_5Zr with a Be_5Au structure [42]). In the static structure factors the change in the TSRO is reflected mainly in the Bhatia–Thornton density–density structure factor $S_{NN}(k)$. The first peak in $S_{NN}(k)$ is rather broad and asymmetric for Zr-rich compounds. It changes to the more symmetrical form characteristic of random close-packing for the Ni-rich alloys [27].

The conclusion as to the similarity of the local order in the crystalline and amorphous phases is also corroborated by investigations of the electronic structure [43–46], which demonstrate a pronounced similarity of the electronic density of states of the crystalline and amorphous phases.

3. Calculation of the vibrational spectrum

3.1. Direct diagonalization

The normal modes of vibration of a solid material (crystal, quasicrystal or glass) are given in the harmonic approximation in terms of the eigenvalues ω_ν and eigenvectors $u_\nu(i)$ of the real- space dynamical matrix (i, j label atomic sites; α, β Cartesian coordinates) [47]

$$D_{\alpha\beta}(ij) = m_i^{-1/2}\Phi\begin{pmatrix} i & j \\ \alpha & \beta \end{pmatrix} m_j^{-1/2} \tag{2}$$

with the force constants $\Phi\binom{i\,j}{\alpha\,\beta}$ being determined by the first and second derivatives of the interatomic pair potentials. The vibrational spectrum (or 'phonon' density of states) $g(\omega)$ may be calculated in terms of the statistics of the eigenvalues ω_ν^2; a Bloch spectral function $f_e(k, \omega)$ for propagating collective excitations with wavevector k and polarization e is given by the projection of the atomic displacements (described by the eigenvectors $u_\nu(i)$) onto a plane wave $e e^{ik\cdot R_i}$ (k vectors are restricted to values compatible with the periodic boundary conditions of the model)

$$f_e(k,\omega) = -\frac{2\omega}{\pi}\sum_\nu \sum_{i,j} e\cdot u_\nu(i) e^{-ik\cdot R_i} e\cdot u_\nu(j) e^{ik\cdot R_j}\delta(\omega^2-\omega_\nu^2). \tag{3}$$

Localization of vibrational eigenmodes is characterized by the participation ratio [48] p_ν

$$p_\nu = \left(\frac{\sum_j |u_\nu(j)|^2}{m_j}\right)\left(\frac{N\sum_j |u_\nu(j)|^4}{m_j^2}\right)^{-1}. \tag{4}$$

For extended modes in crystals one has $p \sim 0.6$; for a mode localized on a single atom, $p_\nu \sim 1/N$.

Calculation of the vibrational eigenmodes by direct diagonalization is limited by computer capacity. In practice, the limit is $N \sim 1000$ atoms. For larger systems, approximate techniques for the calculation of the vibrational spectrum must be developed.

3.2. Recursion calculation

Experimentally, the information on the vibrational eigenmodes is contained in the double-differential scattering cross section for neutrons per solid angle and energy [49]. The coherent cross section is proportional to the dynamical structure factor $S(\boldsymbol{k}, \omega)$:

$$\frac{\mathrm{d}^2\sigma}{\mathrm{d}\Omega\,\mathrm{d}\omega} = \langle b \rangle^2 \left| \frac{k_{\mathrm{out}}}{k_{\mathrm{in}}} \right| S(\boldsymbol{k}, \omega) \tag{5}$$

where $\boldsymbol{k} = \boldsymbol{k}_{\mathrm{in}} - \boldsymbol{k}_{\mathrm{out}}$ is the wavevector difference between the incoming and scattered neutrons and b is the scattering length of the atomic nucleus; $S(\boldsymbol{k}, \omega)$ may be expressed in terms of the vibrational Green function $G_{\alpha,\beta}(ij, \omega)$ defined as the resolvent operator [47]

$$G_{\alpha\beta}(ij, \omega^2) = \left[\omega^2 \delta_{ij}\delta_{\alpha\beta} - D_{\alpha\beta}(ij)\right]^{-1}. \tag{6}$$

In a one-phonon approximation one has

$$S(\boldsymbol{k}, \omega) = -2\hbar[n(\omega) + 1]\mathrm{e}^{-2W(\boldsymbol{k})} \sum_{ij} \mathrm{e}^{-\mathrm{i}\boldsymbol{k}\cdot(\boldsymbol{R}_i - \boldsymbol{R}_j)} - \lim_{\delta \to 0} \sum_{\alpha,\beta} k_\alpha \,\mathrm{Im}\, G_{\alpha\beta}[ij, (\omega + \mathrm{i}\delta)^2]k_\beta \tag{7}$$

where $W(\boldsymbol{k})$ is the Debye–Waller factor and $n(\omega)$ the Bose–Einstein occupation function. It follows immediately that the Bloch spectral function (3) is a diagonal matrix element of the Green function between plane waves [9, 10, 47]:

$$f_e(\boldsymbol{k}, \omega) = -\frac{2\omega}{\pi} \lim_{\delta \to 0} \sum_{i,j} \sum_{\alpha,\beta} e_\alpha \mathrm{e}^{-\mathrm{i}\boldsymbol{k}\cdot\boldsymbol{R}_i}\, \mathrm{Im} G_{\alpha\beta}[ij, (\omega + \mathrm{i}\delta)^2] e_\beta \mathrm{e}^{\mathrm{i}\boldsymbol{k}\cdot\boldsymbol{R}_j} \tag{8}$$

and that the dynamical structure factor $S(\boldsymbol{k}, \omega)$ is given in a one-phonon approximation in terms of the spectral function for longitudinal polarization ($\boldsymbol{e} \| \boldsymbol{k}$) as

$$S(\boldsymbol{k}, \omega) = \frac{\hbar}{m} \frac{n(\omega) + 1}{\omega} \mathrm{e}^{-2W(\boldsymbol{k})} (\boldsymbol{e} \cdot \boldsymbol{k})^2 f_e(\boldsymbol{k}, \omega). \tag{9}$$

Diagonal matrix elements of the Green function (6) may be calculated using the real-space recursion technique [32, 33], i.e. by transforming the dynamical matrix to a basis (constructed via an iterative procedure) where it acquires a tridiagonal form. The diagonal matrix elements are then calculated in terms of a continued-fraction expansion. For the calculation of a Bloch spectral function, the starting state for the construction of the recursive basis is just a plane wave [10]. The vibrational density of states may be calculated by integrating the spectral functions over a large volume in $\boldsymbol{k}$ space or by calculating the imaginary part of the Green function for an initial state with random atomic displacements [10]. The integration in $\boldsymbol{k}$ space corresponds closely to the experimental determination of $g(\omega)$ for polycrystalline or glassy materials [50], but the random-vector approach is computationally more convenient. In practice, up to 60 recursion steps are calculated exactly, corresponding to as many exact eigenvalues. A continuous spectrum is obtained by terminating the continued fraction using the method proposed by Lucchini and Nex [51]. For details of the technique see [10, 33].

For simplicity, (5)–(9) have been formulated for a monatomic material. For a binary system, partial vibrational spectral functions $f_e^{IJ}(\boldsymbol{k}, \omega)$ (I, J = A, B), may be defined

by restricting the atomic displacements to the sites occupied by one atomic species. Partial dynamical structure factors $S_{IJ}(k,\omega)$ are obtained by multiplying the $f_e^{IJ}(k,\omega)$ for longitudinal polarization with the thermal occupation and Debye–Waller factors:

$$S_{IJ}(k,\omega) = \hbar \frac{n(\omega)+1}{\omega} \frac{e^{-W_I(k)}}{m_I^{1/2}} \frac{e^{-W_J(k)}}{m_J^{1/2}} (e\cdot k)^2 f_e^{IJ}(k,\omega). \tag{10}$$

The total dynamical structure factor is given in terms of a weighted average over the partials

$$\langle b\rangle^2 S(k,\omega) = \left[c_A b_A^2 S_{AA}(k,\omega) + c_B b_B^2 S_{BB}(k,\omega) + 2\sqrt{c_A c_B} b_A b_B S_{AB}(k,\omega)\right] \tag{11}$$

with $\langle b\rangle = c_A b_A + c_B b_B$. Alternatively, the partial dynamical structure factors relating to fluctuations in the number density $S_{NN}(k,\omega)$, the concentration $S_{CC}(k,\omega)$ and their cross-correlations $S_{NC}(k,\omega)$ may be used [10]. In practice the 'diagonal' spectral functions f_e^{AA}, f_e^{BB}, f_e^{NN} are calculated using the recursion method, the off-diagonal terms are given by linear combinations of the diagonal terms. The partial Debye–Waller factors $W_I(k)$ may be calculated in terms of the partial vibrational densities of states $g_I(\omega)$, and this completes the information necessary for the determination of $S_{IJ}(k,\omega)$.

The recursion approach to the dynamical properties is closely related to the equation-of-motion (EOM) method [52]. The EOM method in turn may be considered as the harmonic approximation to a full MD calculation. The main advantage of the recursion technique is that it works directly in the wavenumber/energy representation and avoids the cumbersome double Fourier transform from the time-dependent correlation functions to the dynamic structure factors. Moreover, the method is computationally much more convenient: the computational effort for one recursion step is equal to that for one MD step but only $\leqslant 100$ recursion steps are necessary to achieve a resolution in ω that can be achieved only via EOM or MD runs with a minimum of $\sim 10^4$ MD steps (but separate recursion calculations are necessary for every k vector).

4. Phonons in amorphous Ni–Zr alloys

4.1. Partial vibrational spectral functions

Figure 1 shows the partial dynamical spectral functions for amorphous $Ni_{65}Zr_{35}$ and $Ni_{25}Zr_{75}$ alloys for longitudinal excitations propagating along an arbitrary direction in k space, calculated for values of $|k|$ compatible with the periodic boundary conditions. For both alloys we find the familiar result of sharply defined peaks in $f_e^{IJ}(k,\omega)$ in the long-wavelength regime, broadening very rapidly with increasing wavevector (for large $|k|$, $f_e^{IJ}(k,\omega)$ approaches its incoherent limit, i.e. $f_e^{II}(k,\omega) \to g(\omega)$ and $f_e^{IJ}(k,\omega) \to 0$ for $I \neq J$).

For the Zr-rich alloys, the dynamics of the Ni ions has very much the character of localized dispersionless impurity vibrations. Ni ions are only very weakly coupled to the propagating low-frequency modes. The Zr spectral function shows the form familiar from the simple-metal glasses with a rather well defined dispersion relation (defined in terms of the maxima of the spectral functions) passing through a maximum at the pseudo-Brillouin-zone boundary and a minimum near the peak in the partial static structure factor. The SRO seems to be of little consequence for the dynamical properties.

This is different for the Ni-rich alloy. Here both Ni and Zr atoms participate in the long-wavelength 'acoustic' modes, but the form of the partial spectral functions is more

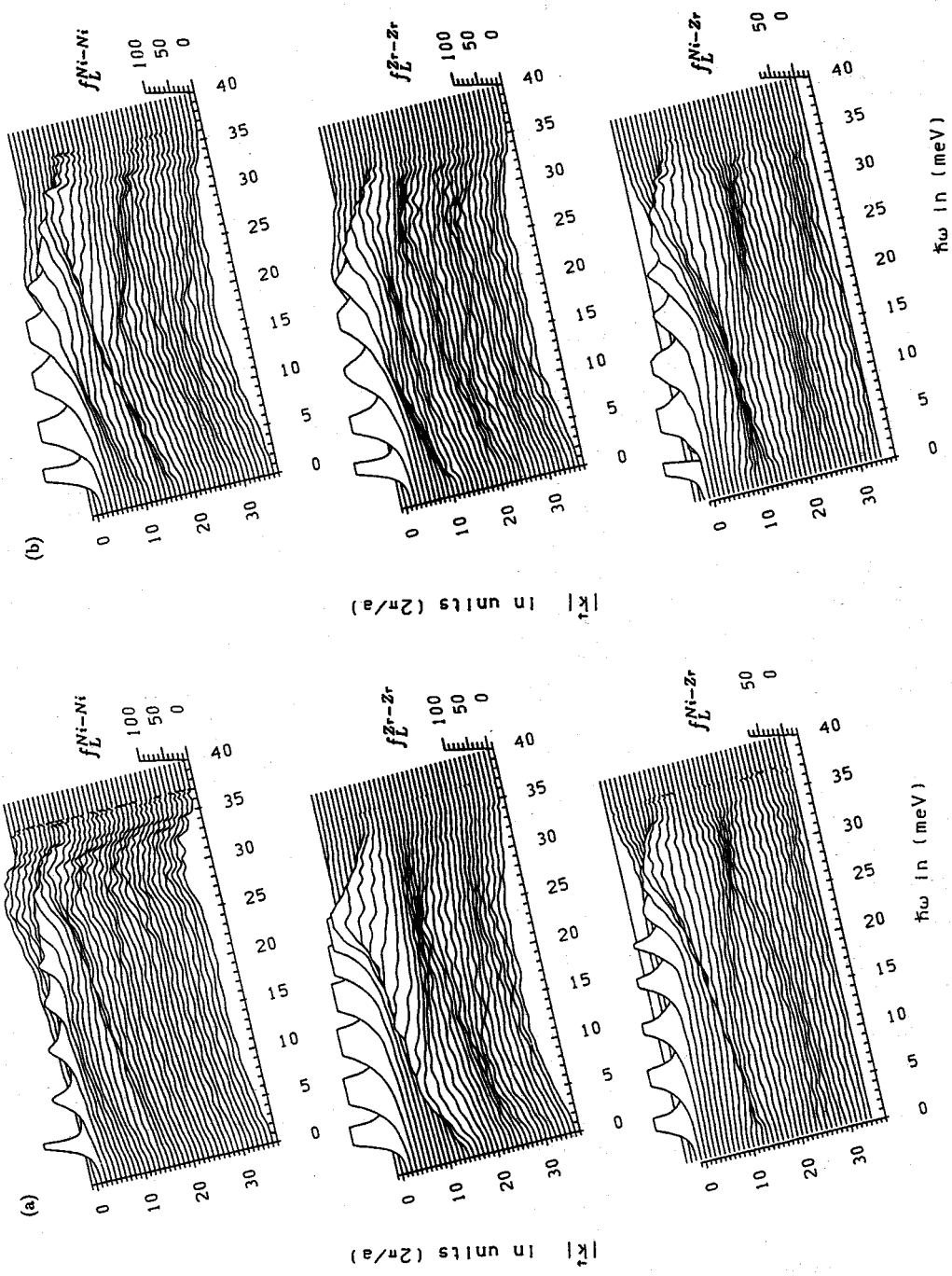

Figure 1. Partial vibrational spectral functions $f_L^{IJ}(k,\omega)$ (in arbitrary units) for propagating longitudinal modes ($e \parallel k$) in amorphous $Ni_{25}Zr_{75}$ (*a*) and $Ni_{65}Zr_{35}$ (*b*) alloys. Wavenumbers are given in units of $(2\pi/a)$ where a is the length of the cubic 2916-atom cell ($a = 39.01$ Å for $Ni_{25}Zr_{75}$, $a = 35.44$ Å for $Ni_{65}Zr_{35}$). The graphs are truncated at a maximum intensity of 100 (in arbitrary units).

complex: in both f^{Ni-Ni} and f^{Zr-Zr} a broad high-frequency peak appears in the $q \to 0$ limit, accompanied by a corresponding minimum in f^{Ni-Zr}. This is the manifestation of 'optic' long-wavelength vibrations with unlike atoms moving out of phase. For larger k, the frequency of the 'optic' modes decreases to a minimum at wavevectors corresponding to the position of the prepeak in the partial static structure factor. At these wavenumbers the spectral functions show a high-frequency 'acoustic' and a low-frequency 'optic' peak (we should remember that these qualifications are strictly legitimate only for crystals; for an attempt to better characterize optic and acoustic modes by diagonalizing the matrix of the second moments of the f^{IJ}, see [10]). At still higher wavenumbers it is impossible to distinguish optic and acoustic modes.

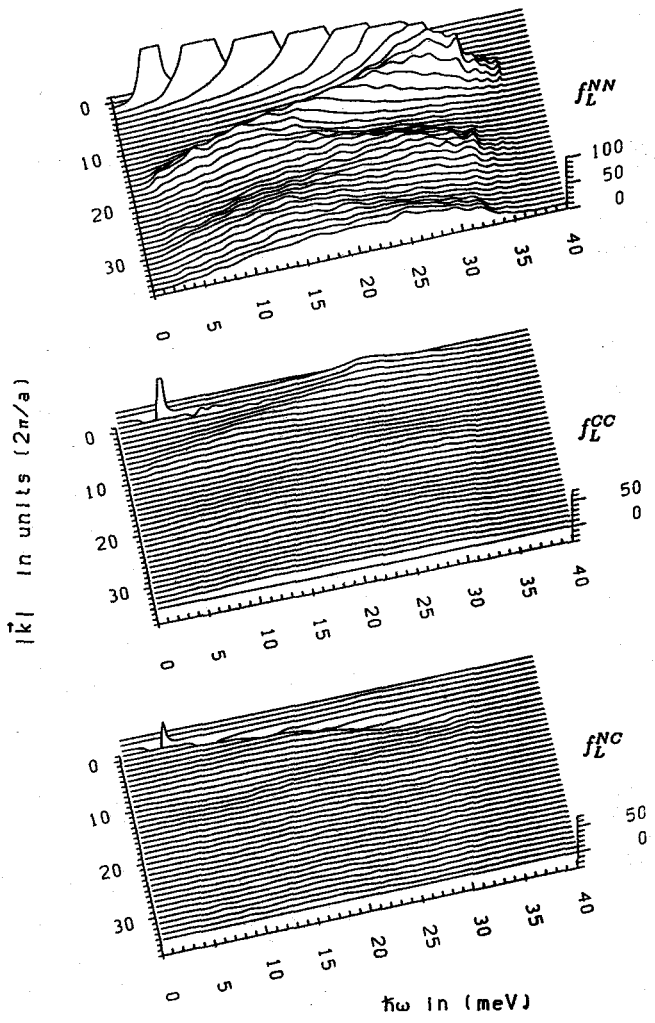

Figure 2. Partial vibrational spectral functions $f_L^{NN}(k,\omega)$, $f_L^{cc}(k,\omega)$ and $f_L^{Nc}(k,\omega)$ for propagating longitudinal density and concentration fluctuations in amorphous $Ni_{65}Zr_{35}$. See also figure 1 and text.

There is a certain correlation between the optic vibrations and non-diffusive dynamical concentration fluctuations. This is illustrated in figure 2 in the example of the Bhatia–Thornton spectral functions f^{NN}, f^{cc} and f^{NC} for a-$Ni_{65}Zr_{35}$. The spectral functions for dynamical density fluctuations show a series of peaks defining dispersion relations for

propagating density modes. The spectral functions for dynamical concentration fluctuations, on the other hand, are rather diffuse; a dispersion relation can be followed only to rather low wavenumbers.

Structural correlations in the dynamics are more distinctly expressed in the partial dynamical structure factors.

4.2. Partial dynamical structure factors

The partial dynamical structure factors $S_{IJ}(k,\omega)$ for three amorphous Ni_xZr_{100-x} alloys with $x = 25, 50, 65$ are shown in figure 3. The $S_{IJ}(k,\omega)$ are calculated from the vibrational spectral functions according to (10), the data are normalized such that $\lim_{k\to\infty} S_{IJ}(k,\omega) = \delta_{IJ}$ and $\lim_{\omega\to 0} S_{IJ}(k,\omega) = S_{IJ}(k)$. The static structure factors from the MD simulation are shown for comparison. Note that the recursion calculation of the spectral functions proceeds in the constant-k mode and that an appropriate terminator has to be chosen for every k. This leads to a certain noise after conversion to a constant-ω representation. Moreover, $\lim_{\omega\to 0} S_{IJ}(k,\omega)$ leads to partial static structure factors for a single metastable equilibrium configuration in the $T \to 0\,\mathrm{K}$ limit, whereas $S_{IJ}(k)$ from the MD simulation represent an ensemble average over a large number of $T = 300\,\mathrm{K}$ configurations.

At low frequencies, $S_{IJ}(k,\omega)$ is very close to the corresponding static structure factor (note in particular the existence of strong CSRO prepeaks, especially in the Ni–Ni structure factors) and shows in addition a sharp sound-wave peak at small k. With increasing frequency the sound-mode peak is shifted to larger k, whereas the main structural peak and the CSRO prepeak shift to smaller k and are strongly damped at intermediate frequency. The CSRO peak crosses the sound-wave peak at $\hbar\omega \geqslant 15\,\mathrm{meV}$, and becomes a broad long-wavelength 'optic' peak at higher frequency. At even higher frequencies the main structural mode increases again in amplitude and merges with the sound-wave peak. At the same time, well defined higher-order peaks develop in all three $S_{IJ}(k,\omega)$. The first peak in the high-frequency dynamic structure factor occurs close to $Q_p/2$, indicating that in the high-frequency modes, next-nearest neighbours move in phase, as for zone-boundary acoustic modes in crystals. The existence of higher-order peaks shows that the structural correlations are well defined in the low-frequency limit and also (more surprisingly) in the high-frequency limit, whereas they are overdamped at intermediate frequencies. However, the structural features characteristic for CSRO are missing in the high-frequency limit.

It is also interesting to have a brief look at the dynamical Bhatia–Thornton structure factors. $S_{NN}(k,\omega)$ and $S_{cc}(k,\omega)/c_{Ni}c_{Zr}$ for $Ni_{50}Zr_{50}$ are shown in figure 4. The variation of $S_{NN}(k,\omega)$ with frequency follows the pattern established for monatomic glasses [11, 12]: with increasing frequency the main structural peak is first progressively broadened and split into two subpeaks. At still higher frequency, the amplitude of these peaks grows again; the positions shift in such a way that for the highest frequencies $S_{NN}(k,\omega)$ is just exactly out of phase with the static $S_{NN}(k)$. The sound-wave peak and the main structural peak merge at high ω. In the dynamical concentration-fluctuation structure factor $S_{cc}(k,\omega)$ there is no sound-wave peak (apart from spurious resonance effects). Again, the main peak in $S_{cc}(k,\omega)$ (whose amplitude in the static limit scales with the degree of CSRO) is damped and split into two subpeaks with increasing frequency. $S_{cc}(k,\omega)$ is almost flat at $\hbar\omega \sim 15\,\mathrm{meV}$. At even higher frequencies the amplitude grows again. The low-k peak represents the high-frequency long-wavelength dynamical concentration fluctuations ('optic' modes). The high-k part merges close to Q_p (for $S_{NN}(k)$!) with a peak issuing from the second peak in $S_{cc}(k)$. This peak represents dynamical concentration fluctuations with a wavelength comparable to the mean interatomic distance $d \sim 2\pi/Q_p$.

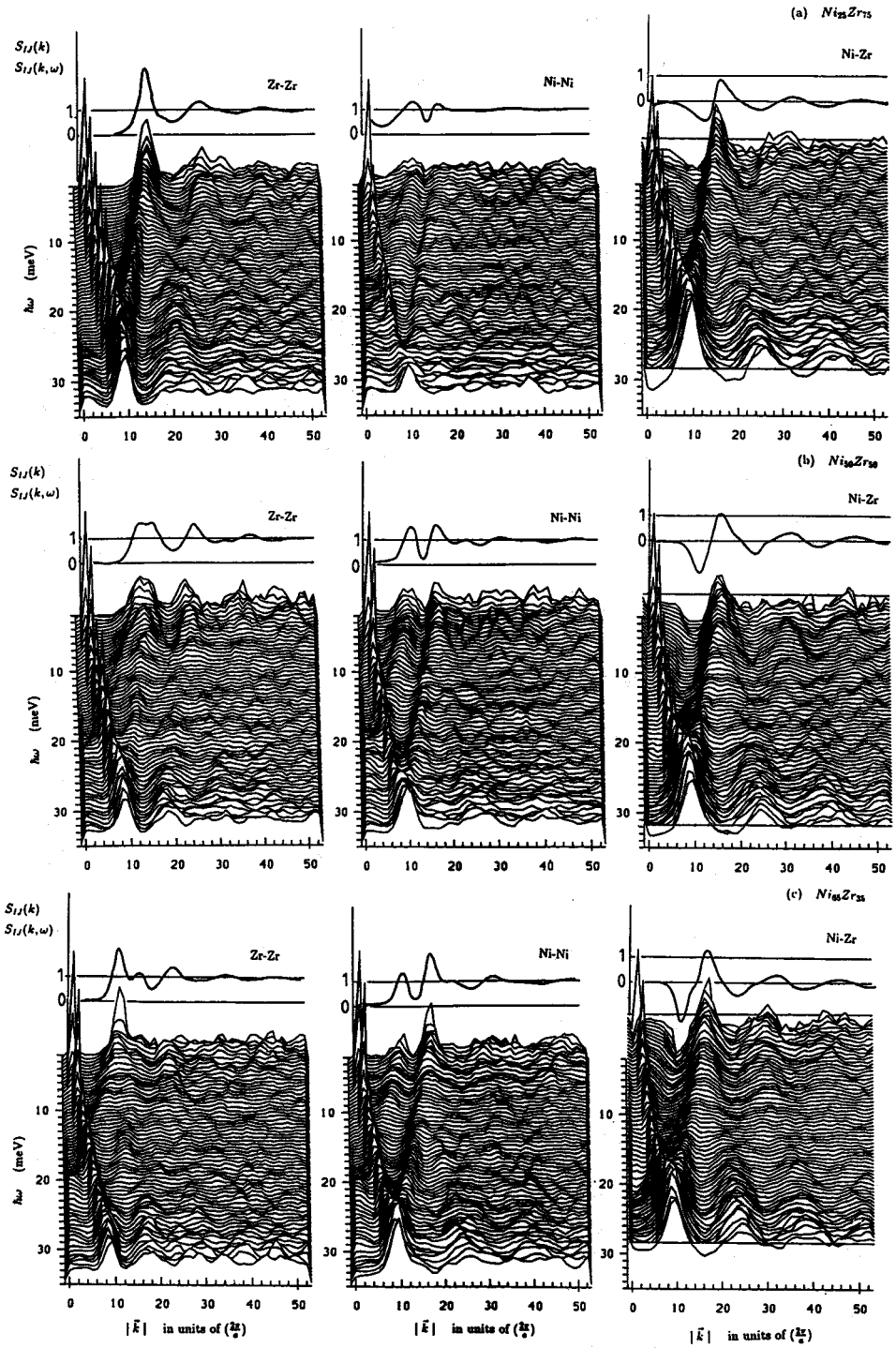

Figure 3. Partial dynamical structure factors $S_{IJ}(k,\omega)$ for amorphous Ni_xZr_{100-x} alloys ((*a*) $x = 25$, (*b*) $x = 50$, (*c*) $x = 65$). $S_{IJ}(k,\omega)$ has been normalized such that $S_{IJ}(k,\omega) \to \delta_{IJ}$ for $k \to \infty$. The partial static structure factors from the MD simulation are shown for comparison. Wavenumbers are given in units of $(2\pi/a)$ where a is the length of the 2916-atom cell (see figure 1).

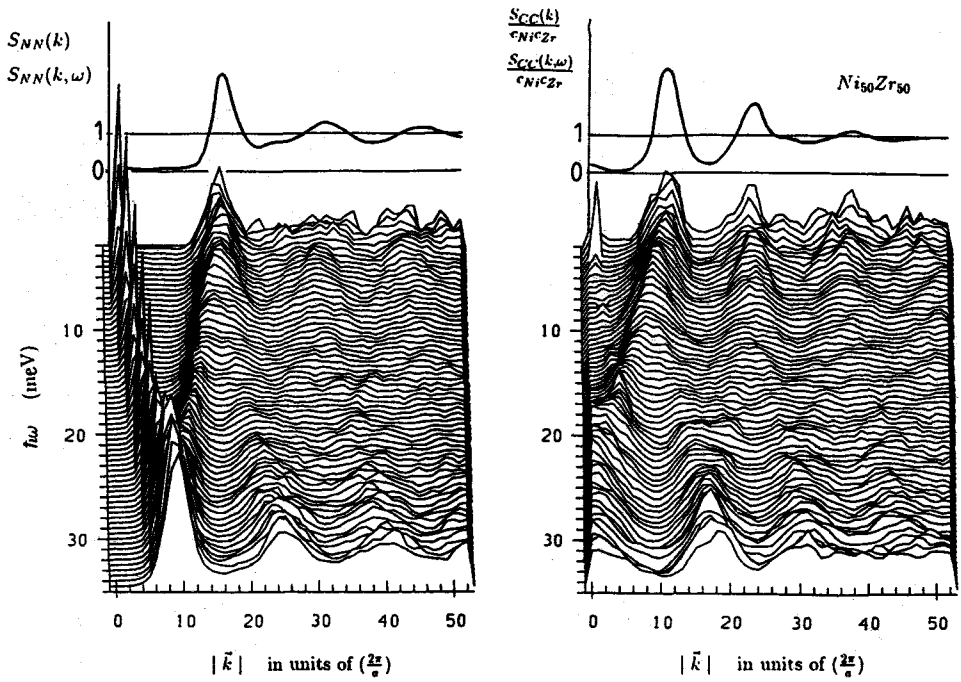

Figure 4. Partial dynamical Bhatia–Thornton structure factors $S_{NN}(k,\omega)$ and $S_{cc}(k,\omega)/(c_{Ni}c_{Zr})$ for amorphous $Ni_{50}Zr_{50}$. See figure 3.

The existence of such well defined high-frequency concentration and density modes is certainly quite surprising. The possibility of an experimental observation of the concentration modes will depend crucially on the neutron-scattering lengths weighting the contributions from the individual $S_{IJ}(k,\omega)$.

Similar calculations may be performed for transverse modes. As has been shown for simple metal glasses, the vibrational spectral functions for transverse modes are well defined only within a rather narrow k-range and converge rapidly to the incoherent limit beyond.

4.3. Dispersion of phonons in glasses

In crystals, the dispersion relations for phonons are determined by the k-dependence of the eigenvalues of the dynamical matrix, or otherwise, in terms of the positions of the poles in the vibrational spectral functions. This definition may be extended to glasses where the δ-function peaks of the spectral functions are replaced by broad maxima: figure 5 shows a dispersion relation for phonons in amorphous $Ni_{50}Zr_{50}$. 'Acoustic phonons' are defined in terms of the maxima in $S_{NN}(k,\omega)$. The dispersion of acoustic phonons shows the now well established 'diffuse-Umklapp' minimum near Q_p. The dispersion of optic phonons is defined in terms of the maxima in $S_{cc}(k,\omega)$. It has a maximum at $k=0$ and may be followed into a minimum near $k \sim Q_p/2$.

In experiments, dispersion relations are usually derived from the maxima in $S(k,\omega)$. Because of the finite width of the spectral functions, multiplication with $(n(\omega)+1)/\omega \propto \omega^2$ for low ω shifts the position of the maximum to lower frequencies. However, this shift is the consequence of the thermal occupation factor and does not represent a change in the frequencies of the eigenmodes.

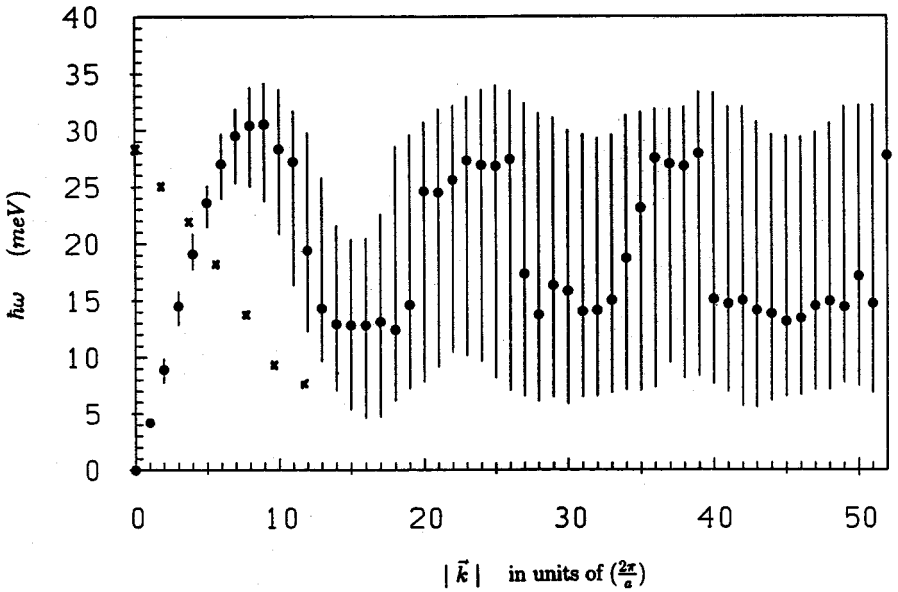

Figure 5. Dispersion relations for propagating collective excitations ('acoustic and optic phonons') in amorphous $Ni_{50}Zr_{50}$. The full dots represent the positions of the maxima in $S_{NN}(k, \omega)$, the bars the full width at half maximum. The crosses represent maxima in $S_{cc}(k, \omega)$. See text.

4.4. Inelastic neutron scattering intensities

The weighted averages of the $f_L^{IJ}(k, \omega)$ and $S_{IJ}(k, \omega)$ according to (10) and (11) define the composite spectral function $F(k, \omega)$ and the one-phonon dynamical structure factor $S(k, \omega)$; they are given for a-$Ni_{25}Zr_{75}$ and a-$Ni_{65}Zr_{35}$ in figures 6 and 7. A dispersion relation defined in terms of the maxima of $F(k, \omega)$ follows closely that derived from the maxima in $f^{NN}(k, \omega)$, apart from minor differences associated with the different weights of the partials depending on the scattering lengths, masses and composition. In a-$Ni_{25}Zr_{75}$, for example, the high-frequency maximum at $k \sim 1.8$–$2.6\,\text{Å}^{-1}$ represents the contribution of Ni vibrations (cf. figure 1(*a*)). Conversion to $S(k, \omega)$ completely changes the picture: multiplication with k^2 nearly completely suppresses the intensity from long-wavelength modes, multiplication with the Bose occupation factor strongly reduces the intensity of the high-frequency modes (note that, in the low-frequency limit, $[n(\omega) + 1]/\omega \propto \omega^{-2}$). For a-$Ni_{25}Zr_{75}$, $S(k, \omega)$ has been measured [34] by inelastic neutron scattering for wavenumbers around Q_p. These results are included in figure 6(*b*); they are in reasonable agreement with the results of the recursion calculations. Minor discrepancies for $\hbar\omega \leqslant 2$–3 meV arise from the finite size of the model and the termination of the continued-fraction expansion. The diameter of the model, together with the range of interatomic forces, restricts the number of recursion levels that can be used without emphasizing the effect of the periodic boundary conditions (see [9] for a more detailed discussion). With only 50–60 exact recursion levels, the exact eigenvalues are rather widely spaced near the edges of the spectrum. Even after extrapolation the continued fraction in the termination procedure, a spurious structure appears in the low- and high-frequency limits of the spectral functions. This structure is very weak in $f^{IJ}(k, \omega)$, but it is blown up by multiplication with the Bose occupation

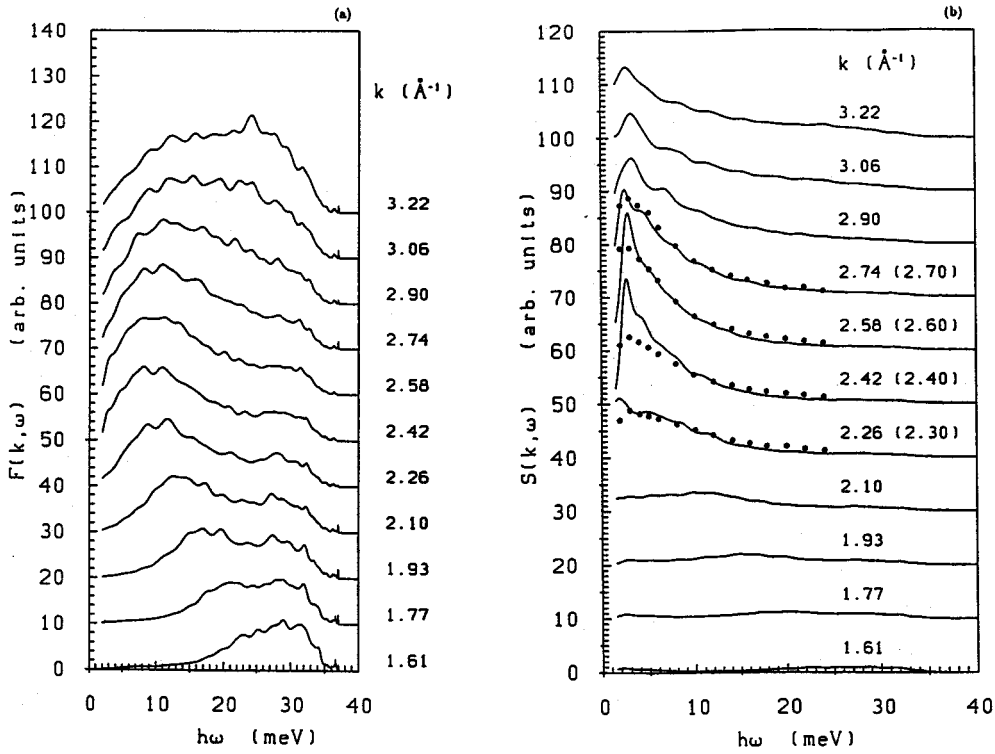

Figure 6. Neutron-weighted composite spectral function $F(k, \omega)$ (*a*) and dynamical structure factor $S(k, \omega)$ in a one-phonon approximation (*b*) for amorphous $Ni_{25}Zr_{75}$. Full curves: theory; dots: inelastic neutron scattering ([34]; the numbers in parentheses give the wavenumbers for which the experiment has been performed).

factor. Similar finite-size effects limiting the low-ω resolution exist also in MD calculations of $S(k, \omega)$.

On the basis of the inelastic neutron scattering data it was concluded that the characteristic eigenmode-frequencies are of the order $\hbar\omega \sim 2$ meV close to the dispersion minimum. The comparison with the calculated dynamical structure factors and spectral functions shows that the characteristic eigenfrequencies in the dispersion minimum are rather of the order $\hbar\omega \sim 10$ meV, but due to the Bose occupation factor the probability that a neutron is scattered by an atomic vibration is much higher for low-energy excitations. This also shows that the high-frequency tail of the neutron-scattering cross section must be measured very accurately in order to yield reliable information on the atomic dynamics in glasses.

Finally, we want to comment briefly on the possibility to extract information on the partial dynamical structure factors by neutron inelastic scattering experiments on isotopically substituted samples. Figures 8 and 9 show the complete neutron-scattering law for one-phonon processes $S(k, \omega)$ in the (k, ω) plane for $Ni_{25}Zr_{75}$ and $Ni_{65}Zr_{35}$ at different isotopic compositions (figures 6 and 7 show the section around $k \sim Q_p$ for natural isotope mixtures, corresponding to parts (*a*) of figures 8 and 9). In principle, the partials $S^{IJ}(k, \omega)$ can be derived from three experiments with a sufficient difference in the weights $w_{IJ} \propto (c_I c_J)^{1/2} b_I b_J$ (cf. equation (11)). Ni alloys are very convenient for such studies, because of the existence of Ni isotopes with positive and negative scattering

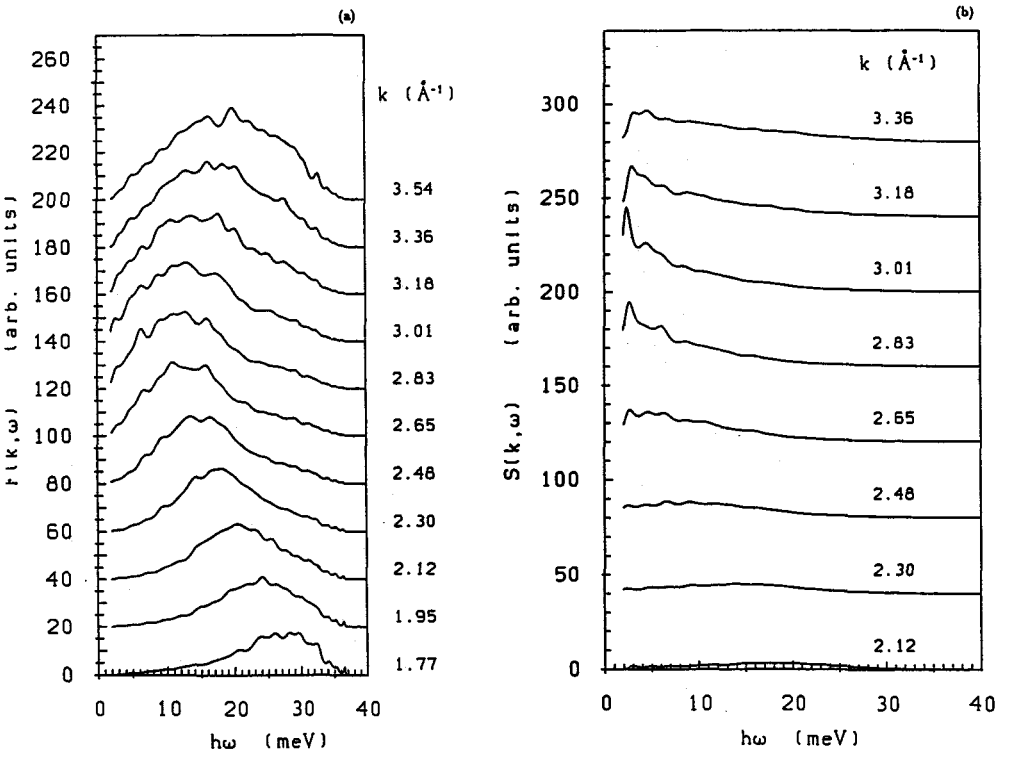

Figure 7. Neutron-weighted composite spectral function $F(k, \omega)$ (*a*) and dynamic structure factor $S(k, \omega)$ (*b*) for amorphous $Ni_{65}Zr_{35}$. See figure 6.

lengths ($b_{Ni}^{58} = 1.44$, $b_{Ni}^{60} = 0.28$, $b_{Ni}^{61} = 0.76$, $b_{Ni}^{62} = -0.87$, $b_{Ni}^{nat} = 1.03$). This ensures a good contrast between experiments performed with isotopically pure Ni^{62} or Ni^{60} (figures 8(*b*) and (*c*)). Still, due to the strong reduction of the intensities at high frequencies, it is doubtful whether the very high accuracy necessary to resolve the partials $S_{IJ}(k, \omega)$ can be achieved, at least at high ω. A direct determination of $S_{ZrZr}(k, \omega)$ or $S_{cc}(k, \omega)$ is possible if zero alloys with either $\bar{b}_{Ni} = 0$ or $\langle b \rangle = 0$ are prepared. However, figures 8(*d*) and 9(*b*), (*c*) demonstrate that due to the combined effects of the Bose occupation factor and of the damping of the $S_{IJ}(k, \omega)$ at intermediate frequencies it will be extremely difficult to explore the structure in the partial dynamical structure factors beyond $\hbar\omega \geqslant 15$ meV. One also has to remember that the resolution of the low-ω maxima will be difficult for most spectrometers because of the overlap of the inelastic $S(k, \omega)$ with the foot of the quasielastic peak.

4.5. Phonon density of states

The total and partial phonon densities of states (DOS) for a series of amorphous Ni_xZr_{100-x} alloys, calculated by taking the average over a series of recursion calculations with random initial states (see section 3.2) are given in figure 10. The results for a-$Ni_{25}Zr_{75}$ are in good agreement with neutron-scattering data on a-$Ni_{24}Zr_{76}$ [34, 54] and very similar to the phonon DOS measured for a-$Cu_{46}Zr_{54}$ [55] and a-Fe_xZr_{100-x} ($x = 33, 40, 80$) [56] alloys. Note that the experiment produces rather a generalized DOS with the partials weighted according to the neutron scattering lengths. For a-$Ni_{24}Zr_{76}$ the normalized weighting factors are 0.508 for Ni and 0.492 for Zr. Therefore the calculated DOS may be compared directly with

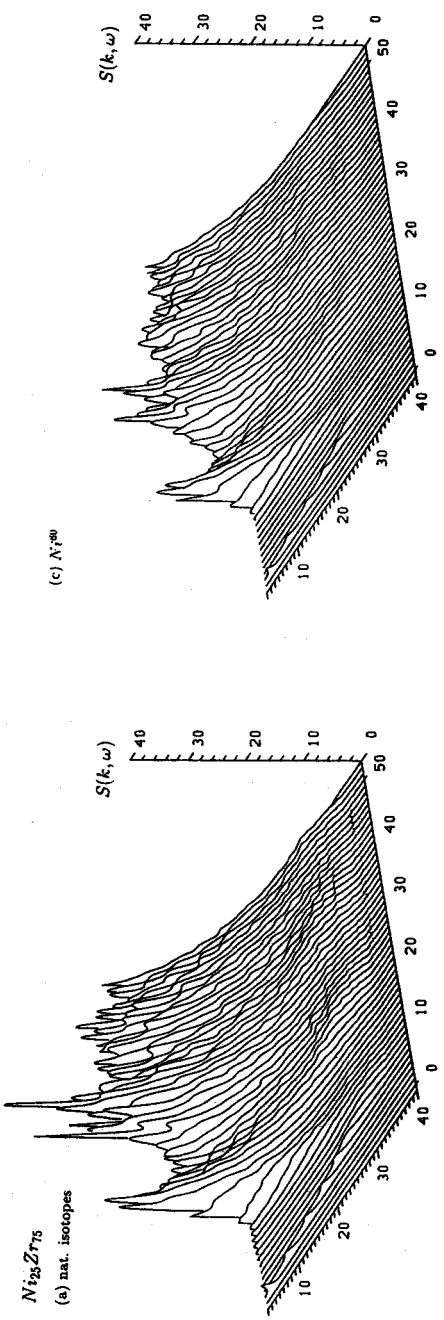

Figure 8. Neutron-scattering law $S(k, \omega)$ for amorphous $Ni_{25}Zr_{75}$ alloys with different isotopic compositions: (*a*) natural isotopic composition ($b_{Zr}^{nat} = 0.71$, $b_{Ni}^{nat} = 1.03$); (*b*) Ni^{62} isotopes ($b_{Ni}^{62} = -0.87$); (*c*) Ni^{60} isotope ($b_{Ni}^{60} = 0.28$); (*d*) Ni-zero alloy with $\overline{b_{Ni}} = 0$. $S(k, \omega)$ is given in arbitrary units, k in units of $(2\pi/a)$ (see figure 1).

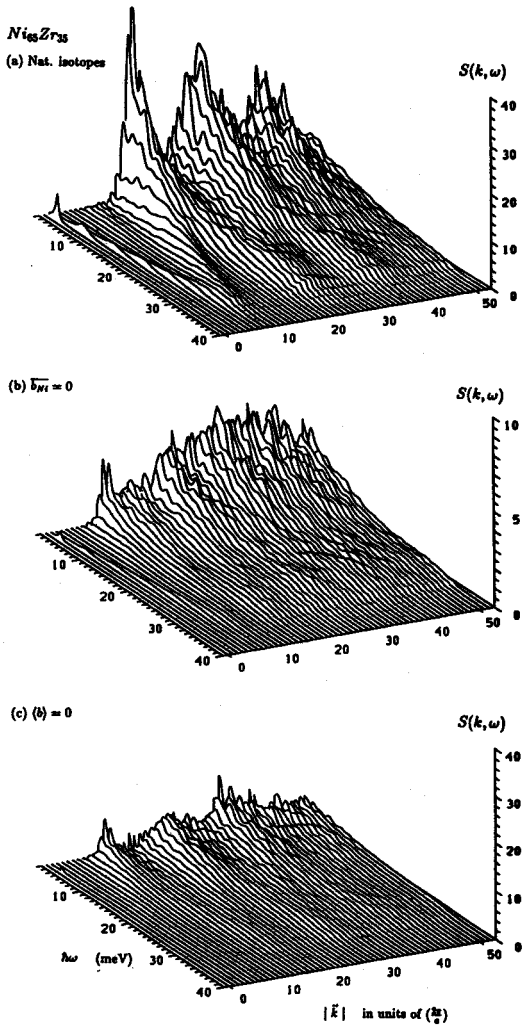

Figure 9. Neutron-scattering law $S(k,\omega)$ for amorphous $Ni_{65}Zr_{35}$ alloys with different isotopic compositions: (*a*) natural isotopic composition, (*b*) Ni-zero alloy with $\overline{b_{Ni}} = 0$, (*c*) zero alloy with $\langle b \rangle = c_{Zr}b_{Zr} + c_{Ni}b_{Ni} = 0$. See also figures 2 and 8.

the experimental data, showing reasonable agreement between theory and experiment. The DOS shows only little variation with composition, apart from a concentration of the Ni contributions at high frequencies at low Ni content.

The most remarkable result is the deviation of the low-frequency part of the DOS from the ω^2 behaviour characteristic for crystalline materials. In the range $2 \leqslant \hbar\omega \leqslant 10$ meV (6 meV for a-$Ni_{25}Zr_{75}$), the DOS varies almost linearly with frequency, i.e. $g(\omega) \propto \omega$. Experimentally [53, 55] $g(\omega) \propto \omega^{4/3}$ has been claimed for $4 \leqslant \hbar\omega \leqslant 8$ meV. The different power law reflects the presence of extra low-energy modes in the glass compared to a crystalline sample of the same composition. At least some of these low-energy modes are not simple propagating Debye phonons (see below). It has also been shown that the number of low-energy modes depends on the preparation of the sample; it is reduced by structural annealing processes [54].

The non-Debye behaviour appears very clearly in a plot of $g(\omega)/\omega^2$ (see the chain curves in figure 10). In this representation the Debye (sound-wave) contribution is a constant. The existence of excess low-energy modes gives rise to a peak in $g(\omega)/\omega^2$ at 2–3 meV, which is

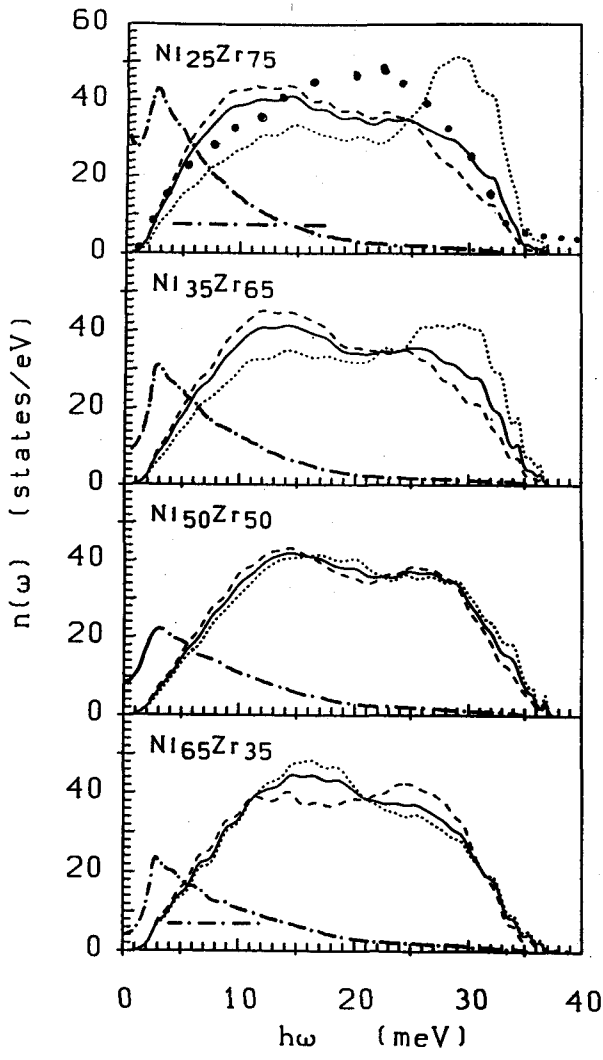

Figure 10. Total and partial phonon densities of states for amorphous Ni_xZr_{100-x} alloys. Full curve: total DOS; broken curve: partial Zr DOS; dotted curve: partial Ni DOS. The full dots show the measured generalized DOS for Ni_{24} Zr_{76} (after [54]). All distributions are normalized to unity. The chain curves show $g(\omega)/\omega^2$, with horizontal lines marking the Debye limits (see text).

often referred to as the 'bosonic' peak. This nomenclature seems to imply that the origin of the excess modes is in quantum effects. However, the 2 meV peak is primarily a structural effect. This follows very clearly by comparing figure 10 with the dynamical structure factors $S(k, \omega)$ shown in figures 6(*b*) and 7(*b*). The strongest contribution to the low-energy peak in $g(\omega)/\omega^2$ comes from $k \sim Q_p$, i.e. from the dispersion minimum due to diffuse Umklapp scattering processes. 'Diffuse Umklapp scattering' means that at these wavevectors the atoms move cooperatively, with a wavelength of the vibrations comparable to the mean interatomic distance. The in-phase movement of the atoms is superposed by small local relaxations. In a crystal such collective movements are possible (at zero energy) if the wavevector coincides with a reciprocal lattice vector and no local relaxations are required. In a glass collective vibrations at low energy are possible over a range of wavelengths, due to the finite width of the peak in the static structure factor. This means that a much larger volume is available in phase space for these low-energy modes in glasses than in crystals. Most of the excess modes are short-wavelength propagating modes (although they

are strongly damped, as demonstrated by the width of $S(k, \omega)$), but some of them may also be localized (see below). The physics expressed by the 'diffuse-Umklapp' model is the same as that described by the 'soft-potential' model [23–25]. The 'soft-potential' model postulates a common origin of the relaxations, soft localized modes and tunnelling modes. A description of tunnelling effects (which are responsible for the thermodynamic anomalies at $T \leqslant 1\,\mathrm{K}$) is outside the scope of our classical treatment of atomic motions, but the manifestations of the excess modes in the thermodynamic properties at high temperatures ($T \geqslant 10\,\mathrm{K}$) are clearly observable.

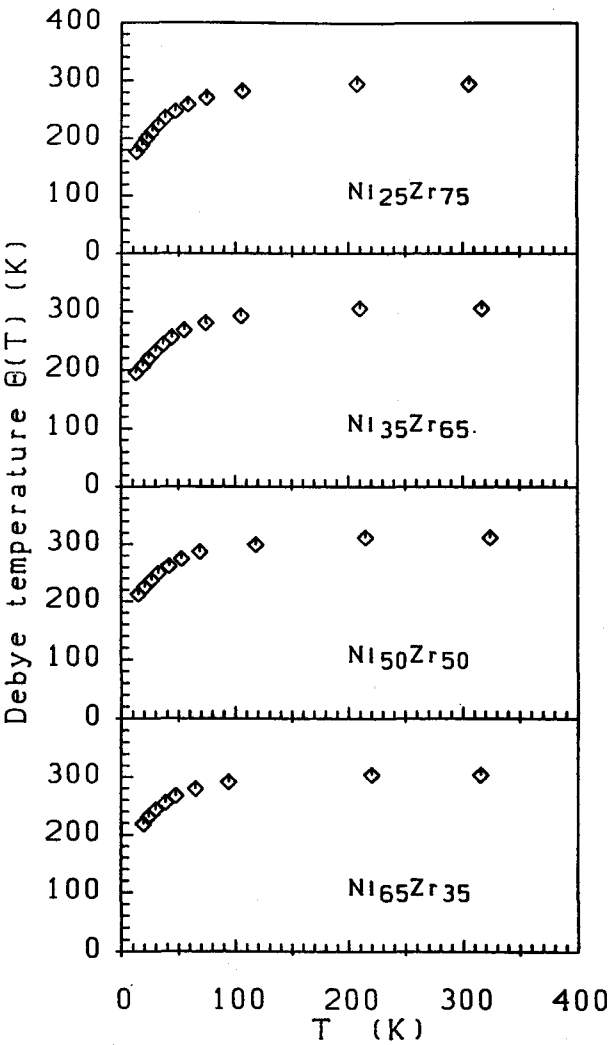

Figure 11. Temperature variation of the effective Debye temperature $\Theta(T)$ fitted to the lattice specific heat of a-Ni_xZr_{100-x} alloys.

Figure 11 shows the effective Debye temperature $\Theta(T)$ for Ni_xZr_{100-x} glasses, fitted to the lattice specific heat C_v obtained from the vibrational DOS. At room temperature we find $\Theta = 249, 305, 312$ and $303\,\mathrm{K}$ at $x = 25, 35, 50$ and 65, which is slightly lower than the mean value of the crystalline metals (Ni: $\Theta = 375\,\mathrm{K}$, Zr: $\Theta = 288\,\mathrm{K}$).

At temperatures between 100 and 20 K, the effective Debye temperature drops to $\Theta \sim 190$–210 K (the higher values corresponding to the lower Ni content), to be compared with experimental values [57] of $\Theta = 235$ K for a-$Ni_{36}Zr_{64}$. The decrease of Θ reflects the presence of excess low-energy excitations in the vibrational spectrum. The position of the 'bosonic' peak corresponds to a temperature of about 20–25 K, characteristic for the range where a maximum in C_v/T^3 and a plateau in the thermal conductivity are observed in many metallic glasses [19–21]. Below this energy, $g(\omega)/\omega^2$ decreases again and this corresponds to an increase in the effective Debye temperature. However, as for our finite models the actual number of modes at these energies is already very small, quantitatively meaningful calculations will require models based on a larger number of atoms.

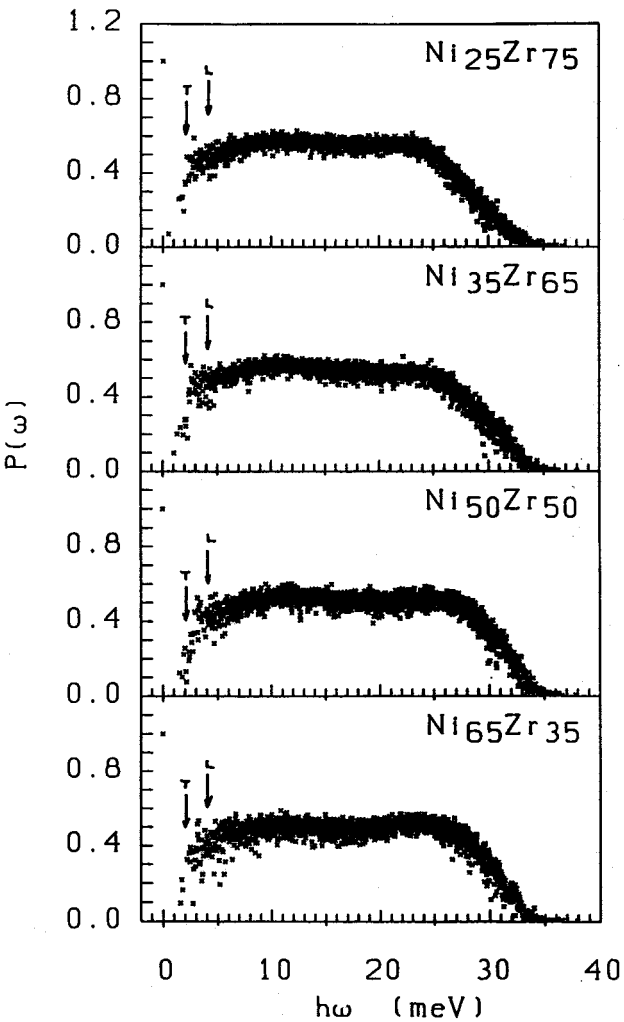

Figure 12. Participation ratio $p(\omega)$ of vibrational eigenmodes in amorphous Ni_xZr_{100-x} alloys. The vertical arrows marked T and L show the low-frequency cut-offs for propagating long-wavelength transverse and longitudinal modes.

4.6. Phonon localization

The participation ratio $p(\omega)$ for vibrational eigenmodes in amorphous Ni_xZr_{100-x} alloys, calculated by direct diagonalization of the dynamical matrix for $N = 729$-atom ensembles,

is shown in figure 12. Three different regimes may be distinguished. (i) For frequencies in the range $10 \leqslant \hbar\omega \leqslant 25$ meV the participation ratio of all modes is close to $p(\omega) \sim 0.5$, i.e. of the same order as for vibrational eigenstates in crystals. Hence all these modes are extended. (ii) For high frequencies ($\hbar\omega > 25$ meV) the participation ratio decreases, reaching very small values of $0.01 \leqslant p(\omega) \leqslant 0.03$ for $\hbar\omega > 34$ meV. In these high-frequency localized modes the amplitude of the atomic vibrations is large only on a very small number of isolated sites, and even these motions are in general uncorrelated. A typical high-frequency localized mode is shown in figure 13(*a*). The atomic sites with the large atomic displacements are characterized by high atomic level stresses [58, 59], in particular by high hydrostatic atomic level pressures. Modes with $25 \leqslant \hbar\omega \leqslant 30$ meV are in the transition regime with increasing localization. (iii) At low frequencies ($\hbar\omega \leqslant 10$ meV) $p(\omega)$ scatters between $p \sim 0.6$ and $p \sim 0.06$, indicating the coexistence of extended and localized modes. Considering somewhat arbitrarily modes with $p < 0.2$ as localized (corresponding to an effective mass of the localized mode of about 20 atomic masses for our model) we find a concentration of about 10^{-3} to 10^{-2} localized modes in the regime $\hbar\omega < 10$ meV, similar to experiments on many glasses [19, 20]. The eigenvectors of a typical low-energy localized mode are shown in figure 13(*b*). A characteristic difference between high- and low-energy localized modes is that while the high-energy modes are usually localized on only one or two atomic sites (corresponding to participation ratios of $p(\omega) \sim 0.01$), the low-energy modes involve a group of atoms (about 10–20) with correlated atomic motions (and hence the participation ratio is larger by typically a factor of ten). Localized single-particle modes would be possible only at a large local concentration of free volume, which is, however, unstable in the densely packed metallic glasses.

Our result that, although there exists a large number of localized high-frequency modes, only very few localized low-frequency modes can be found, illustrates a characteristic difference between electron and phonon localization in disordered solids. The major point is that the characteristic wavelength of low-frequency vibrations is large and therefore scattering from structural imperfections is weak [60]. This is also the reason why it is difficult to assign the origin of the soft localized modes to a particular type of geometrical defect. A negative hydrostatic atomic level pressure shifts the centre of gravity of the local vibrational DOS to low frequencies [59], but this is not a sufficient condition for the existence of a low-frequency localized mode. Some attempts to characterize the geometrical origin of these modes and their relation to the soft-potential model and low-temperature relaxation processes have been made by Schober and Laird [25, 61]. Their results stress the similarity between the atomic motions in the soft localized modes and in jump relaxation processes that occur well below the glass-transition temperature. Our study confirms for the first time the existence of localized low-energy modes in realistic models of metallic glasses, but a detailed investigation of the atomic motions in these modes must be left to future work.

We also have to emphasize that the finite size of our models limits to a certain extent the investigation of low-energy modes. With the diameter of our 729-atom models, the periodic boundary conditions limit the wavevector $\boldsymbol{k}$ to $k_i \geqslant 2\pi/a \sim 0.16$–$0.17$ Å, $i = x, y, z$. Given the minimum wavevector and the longitudinal and transverse velocities of sound (cf. the dispersion relations shown in figure 5), we find cut-off frequencies of $\hbar\omega_{\mathrm{L}}^{\mathrm{cut}} \simeq 4$ meV for longitudinal and $\hbar\omega_{\mathrm{T}}^{\mathrm{cut}} \simeq 2$ meV for transverse long-wavelength modes. These cut-offs are indicated in figure 12. Most localized modes are below these cutoffs. To extend the numerical investigations to larger systems (with lower cut-off frequencies allowing for a coupling of localized and long-wavelength propagating modes) will require the adoption of techniques for the iterative diagonalization of very large matrices.

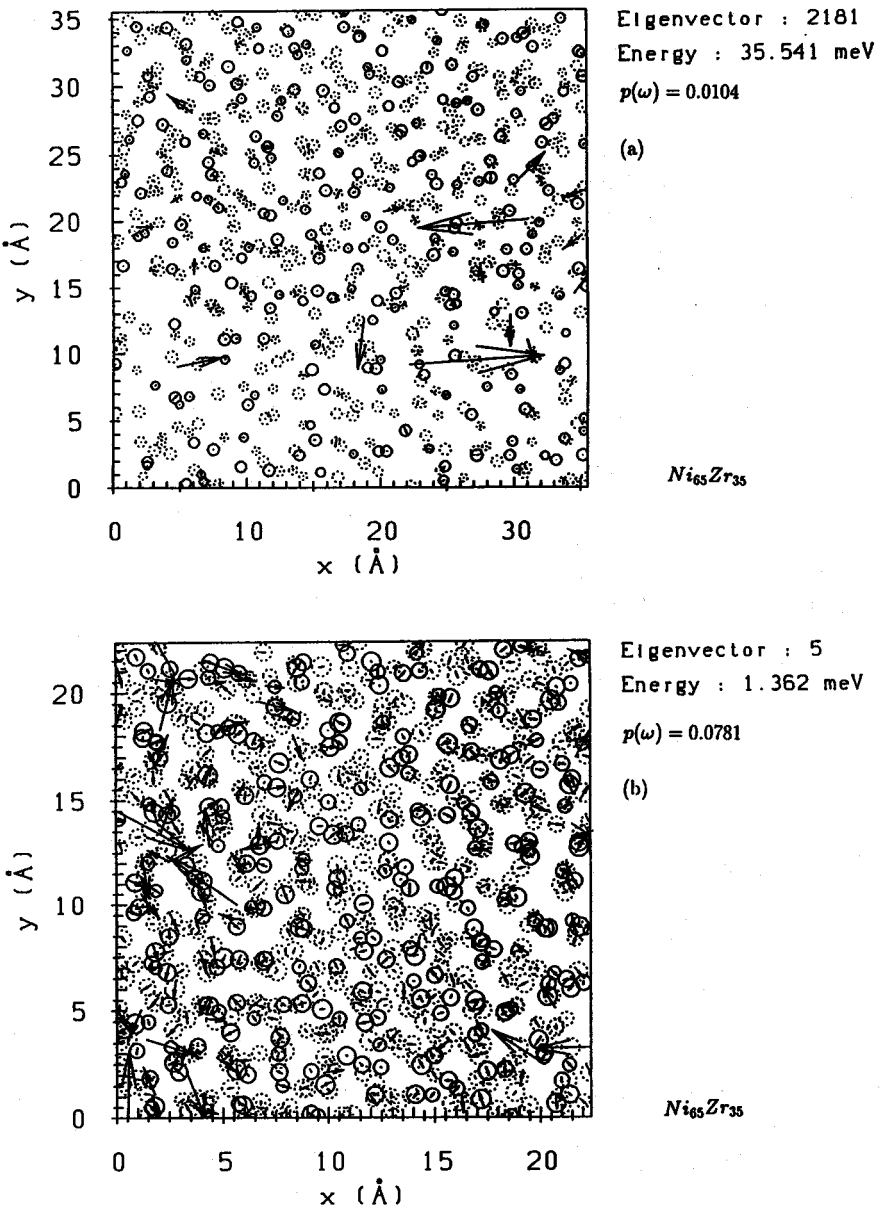

Figure 13. Eigenvectors of a localized high-frequency (*a*) and a localized low-frequency (*b*) mode in a-$Ni_{65}Zr_{35}$. All atoms with $|u_\nu(i)| \geqslant 0.02$ are shown as projections onto the (x, y) plane (full circles: Zr atoms; broken circles: Ni atoms). Eigenvectors (displacement amplitudes) are shown as arrows.

5. Conclusion

We have presented the first investigation of partial dynamic structure factors in metallic glasses with pronounced chemical and topological short-range order. We have shown that the features characterizing the CSRO in the static partial structure factors (prepeaks etc) persist in the dynamic partial structure factors in the low- and high-frequency regimes,

whereas in the intermediate-frequency regime the strong interaction between the vibrational modes leads to a smearing of all structurally induced characteristics. In particular, the peaks in the structure factor $S_{cc}(k, \omega)$ for dynamical concentration fluctuations define a dispersion relation for 'optic' modes with a maximum at $k = 0$ and a minimum near the peak in $S_{cc}(k)$, $k \sim 0.6Q_p$, i.e. just out of phase with the dispersion relation for 'acoustic' modes defined in terms of dynamic density fluctuations.

We have also presented the first investigation of phonon localization in realistic models of metallic glasses. The most important result is the existence of low-frequency localized modes. Although these modes represent only a small fraction of the total vibrational spectrum, they make an important contribution in the low-frequency limit ($\hbar\omega \leqslant 3$ meV) and are hence of decisive importance for the low-temperature thermodynamic properties. Our results support the soft-potential model for the explanation of the low-temperature thermodynamic anomalies of metallic glasses. A structural characterization of the origin of these modes however must be left to future work.

Acknowledgments

Stimulating discussions with Dr J B Suck are gratefully acknowledged. This work has been supported by the Bundesministerium für Wissenschaft und Forschung within the framework of the Materials Research Program, contract No GZ 49.787/2/2-24/92.

References

[1] Suck J B and Rudin H 1983 *Glassy Metals II (Topics in Applied Physics 53)* ed H Beck and H J Güntherodt (Berlin: Springer)
[2] Davidovic M and Soper A K (ed) 1989 *Static and Dynamic Properties of Liquids (Springer Proceedings in Physics 40)* (Berlin: Springer)
[3] Bengtzelius U, Götze W and Sjölander A 1984 *J. Phys. C: Solid State Phys.* **17** 5915
[4] Baym G 1964 *Phys. Rev.* **135** A1691
[5] Hafner J 1985 *J. Non-Cryst. Solids* **69** 3253
[6] Jäckle J and Froböse K 1980 *J. Phys. F: Met. Phys.* **10** 1471
[7] Suck J B, Rudin H, Güntherodt H J and Beck H 1980 *J. Phys. C: Solid State Phys.* **13** L1045
[8] Suck J B, Rudin H, Güntherodt H J and Beck H 1983 *Phys. Rev. Lett.* **50** 49
[9] Hafner J 1983 *Phys. Rev.* B **27** 678
[10] Hafner J 1983 *J. Phys. C: Solid State Phys.* **16** 5773
[11] Grest G S, Nagel S R and Rahman A 1982 *Phys. Rev. Lett.* **49** 1271
[12] Nagel S R, Grest G S and Rahman A 1983 *Phys. Today* **36** 24
[13] Boon J P and Yip S 1980 *Molecular Hydrodynamics* (New York: McGraw-Hill)
[14] Kambayashi S and Kahl G 1992 *Phys. Rev.* A **46** 3255
[15] Hafner J 1981 *J. Phys. C: Solid State Phys.* **14** L287
[16] Bhatia A B and Singh R N 1985 *Phys. Rev.* B **31** 4751
[17] Lewis L J and Ashcroft N W 1986 *Phys. Rev.* B **34** 8477
[18] Anderson P W, Halperin B I and Varma C M 1972 *Phil. Mag.* **25** 1
[19] Phillips W A (ed) 1981 *Amorphous Solids—Low Temperature Properties* (Berlin: Springer)
[20] Phillips W A 1987 *Rep. Prog. Phys.* **50** 1657
[21] Hunklinger S and Raychoudhuri A K 1986 *Prog. Low. Temp. Phys.* **9** 267
[22] Buchenau U, Zhou H M, Nücker N, Gilroy K S and Phillips W A 1988 *Phys. Rev. Lett.* **60** 1368
[23] Nagel S R, Rahman A and Grest G S 1984 *Phys. Rev. Lett.* **53** 368
[24] Buchenau U, Galperin Yu M, Gurevich V L and Schober H R 1991 *Phys. Rev.* B **43** 5039
[25] Schober H R and Laird B B 1991 *Phys. Rev.* B **44** 6746
[26] Steeb S and Lamparter P 1993 *J. Non-Cryst. Solids* **156–158** 24
[27] Hausleitner Ch and Hafner J 1992 *Phys. Rev.* B **45** 115, 128

[28] Hausleitner Ch and Hafner J 1993 *Phys. Rev.* B **47** 5689
[29] Fukunaga T, Hayashi N, Watanabe N and Suzuki K 1985 *Rapidly Quenched Metals V* ed S Steeb and H Warlimont (Amsterdam: North-Holland) p 475
[30] Lefebvre S, Quivy A, Bigot J, Calvayrac Y and Bellissent R 1985 *J. Phys. F: Met. Phys.* **15** L99
[31] Mizoguchi T, Yoda S, Akutsu N, Yamada S, Nishioka J, Suemasa T and Watanabe N 1985 *Rapidly Quenched Metals V* ed S Steeb and H Warlimont (Amsterdam: North-Holland) p 483
[32] Haydock R, Heine V and Kelly M J 1975 *J. Phys. C: Solid State Phys.* **5** 2845
[33] Haydock R 1981 *Solid State Physics vol 35* (New York: Academic) p 216
[34] Suck J B 1985 *Rapidly Quenched Metals V* ed S Steeb and H Warlimont (Amsterdam: North-Holland) p 471
[35] Heine V and Weaire D 1970 *Solid State Physics vol 24* (New York: Academic) p 247
[36] Hafner J 1987 *From Hamiltonians to Phase Diagrams (Solid State Sciences 70)* ed M Cardona and P Fulde (Berlin: Springer)
[37] Sutton A P, Finnis M W, Pettifor D G and Ohta Y 1988 *J. Phys. C: Solid State Phys.* **21** 35
[38] Pettifor D G 1990 *Many-Atom Interactions in Solids* ed R M Nieminen, M J Puska and M H Manninen (Berlin: Springer)
[39] Finnis N W and Sinclair J E 1984 *Phil. Mag.* A **50** 45
[40] Arnold A, Mauser N and Hafner J 1989 *J. Phys.: Condens. Matter* **1** 965
[41] Arnold A and Mauser N 1990 *Comput. Phys. Commun.* **51** 267
[42] Villars P and Calvert L D 1985 *Pearson's Handbook on Crystallographic Data for Intermetallic Phases* (Metals Park, Ohio: American Society for Metals)
[43] Jank W, Hausleitner Ch and Hafner J 1991 *Europhys. Lett.* **16** 473
[44] Turek I, Becker Ch and Hafner J 1992 *J. Phys.: Condens. Matter* **4** 7257
[45] Amamou A, Kuentzler R, Dossmann Y, Forey P, Glimois J L and Feron J L 1982 *J. Phys. F: Met. Phys.* **12** 2509
[46] Oelhafen P 1987 *Liquid and Amorphous Metals* ed E Lüscher, G Fritsch and G Jacucci (Dordrecht: Martinus Nijhoff) p 333
[47] Maradudin A A, Montroll F W, Weiss G W and Ipatova I P 1971 *Theory of Lattice Dynamics in the Harmonic Approximation* (New York: Academic)
[48] Dean P 1972 *Rev. Mod. Phys.* **44** 127
[49] Lovesey S and Springer T 1977 *Dynamics of Solids and Liquids by Neutron Scattering* (Berlin: Springer)
[50] Oskotskii V S 1967 *Sov. Phys.–Solid State* **9** 420
[51] Lucchini M V and Nex C M M 1987 *J. Phys. C: Solid State Phys.* **20** 3125
[52] Alben R, von Heimendahl L, Galison P and Lang M I 1975 *J. Phys. C: Solid State Phys.* **8** L468
[53] Suck J B, Rudin H and Güntherodt H J 1981 *J. Phys. C: Solid State Phys.* **14** 2305
[54] Suck J B 1989 *Dynamics of Disordered Materials (Springer Proceedings in Physics it 37)* ed D Richter, A J Dianoux, W Petry and J Texeira (Berlin: Springer) p 182
[55] Suck J B, Rudin H, Güntherodt H J, Beck H, Daubert J and Gläser W 1980 *J. Phys. C: Solid State Phys.* **13** L167
[56] Gompf F, Reichardt W and Geibel Ch 1985 *Amorphous Metals and Non-Equilibrium Processing* ed M von Allmen (Paris: Editions de Physique) p 293
[57] Mizutani U 1983 *Prog. Mater. Sci.* **28** 97
[58] Egami T, Maeda K and Vitek V 1980 *Phil. Mag.*A **41** 883
[59] Hafner J 1983 *Proc. 2nd Int. Conf. on the Structure of Non-crystalline Solids* ed P H Gaskell, J M Parker and E A Davies (London: Taylor and Francis) p 539
[60] Jäckle J 1981 *Solid State Commun.* **39** 1261
[61] Schober H R and Laird B B 1993 *J. Non-Cryst. Solids* **156–158** 965